

# Non-doped, blue-emitting, color-stable, organic light-emitting diode based on 2,2':6',2''-ternaphthalene

Günther Schwabegger · Theo Dingemans ·  
Roland Resel · Helmut Sitter · Clemens Simbrunner

Received: 23 March 2014 / Accepted: 24 March 2014 / Published online: 27 April 2014  
© The Author(s) 2014. This article is published with open access at Springerlink.com

**Abstract** A novel non-doped blue-emitting material, 2,2':6',2''-ternaphthalene (NNN), which is based on three naphthalene units forming a rodlike molecule, has been synthesized and characterized. Organic light-emitting diodes based on NNN as emitter exhibit blue emission with Commission Internationale de l'Eclairage color coordinates of  $x = 0.18$  and  $y = 0.11$ . In addition, the morphology and crystallographic structure of the NNN thin films has been investigated. NNN deposited on poly[3,4-(ethylene-dioxy) thiophene]:poly (styrene sulfonate) on Indium Tin Oxide-covered glass forms crystalline structures of high crystallographic quality. The molecules are aligned almost perpendicular to the substrate surface and exhibit a tilt angle of  $23^\circ$ .

## 1 Introduction

Since the first reports of organic electroluminescent (EL) devices in the late 1980s [1–4], there has been significant interest in the field of organic light-emitting diodes

(OLEDs) driven by questions related to fundamental research as well as by proposed industrial applications. An example is solid-state lightning [5–7], which holds great promise as an energy-efficient light source. Another example is the use of OLEDs for full color displays [8, 9], which requires red, green and blue emitters of high color purity. As described in a recent review [10], the development of red and green emitters of sufficient quality did not pose too many problems but the performance of blue emitters often suffers from the wide band gap of the used materials. The intrinsically wide band gap leads to difficulties in the band alignment with respect to the electronic levels of other layers in the OLED and thus to limitations in the charge carrier injection and further to a reduced EL efficiency. Another problem related to the issue of a high band gap is the consequence that the lowest unoccupied molecular orbital (LUMO) is close to the vacuum energy level, which reduces the lifetimes of blue OLEDs because the material is susceptible to oxidation. Nevertheless, there are many reports on blue-emitting OLEDs [4, 11–20] and the optimization of device structure as well as the investigation of new blue emitters is still in progress.

In this paper, we present a new naphthalene-based small molecule [2,2':6',2''-ternaphthalene (NNN), see Fig. 1a], which can be used as a blue-emitting active layer in an OLED. We present the electrical and optical device characteristics, as well as the morphological and structural analysis of the evaporated thin films.

## 2 Experimental processing

### 2.1 Synthesis of 2,2':6',2''-ternaphthalene (NNN)

The details of NNN synthesis are reported elsewhere [21].

G. Schwabegger (✉) · H. Sitter · C. Simbrunner  
Institute of Semiconductor and Solid State Physics, Johannes  
Kepler University Linz, Altenbergerstraße 69, 4040 Linz,  
Austria  
e-mail: guenther-schwabegger@gmx.at

C. Simbrunner  
e-mail: clemens.simbrunner@jku.at

T. Dingemans  
Faculty of Aerospace Engineering, Delft University of  
Technology, Kluyverweg 1, 2629 HS Delft, The Netherlands

R. Resel  
Institute of Solid State Physics, Graz University of Technology,  
Petersgasse 16, 8010 Graz, Austria

**Fig. 1** **a** Chemical structure of 2,2':6',2''-ternaphthalene. **b** Sketch of the OLED device structure

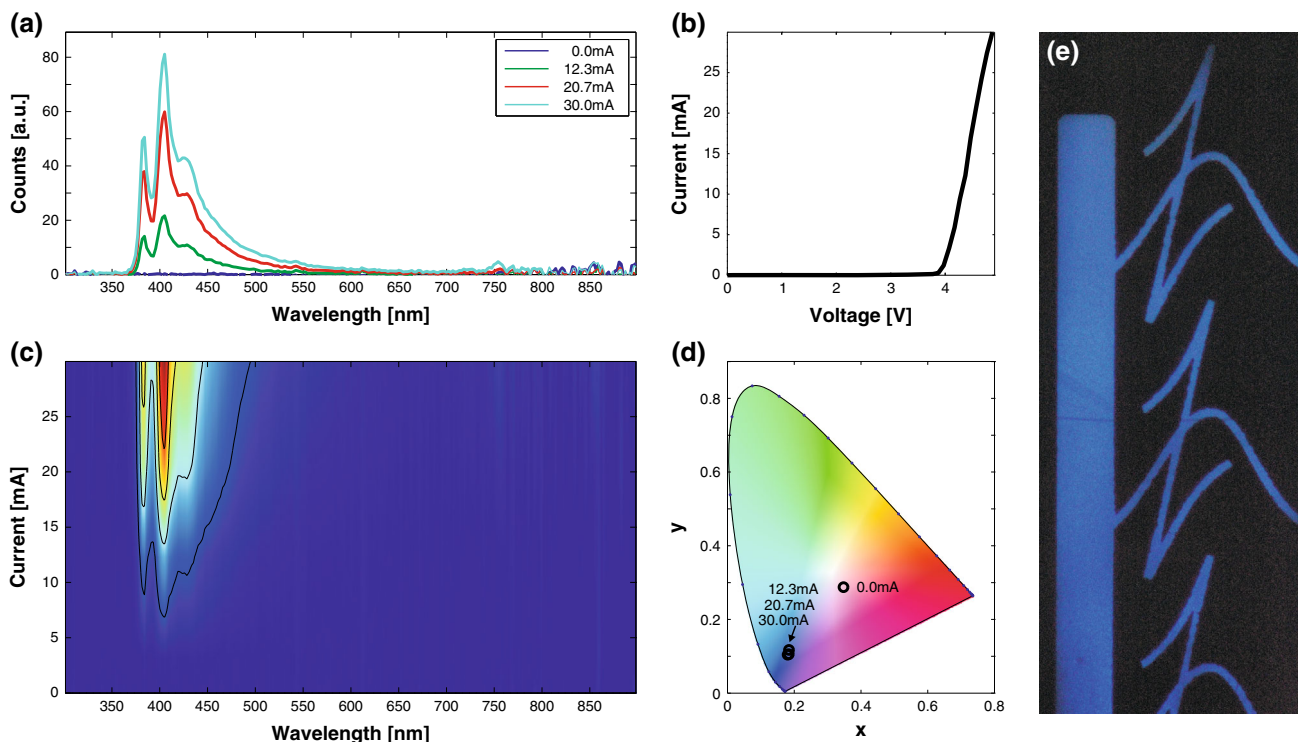
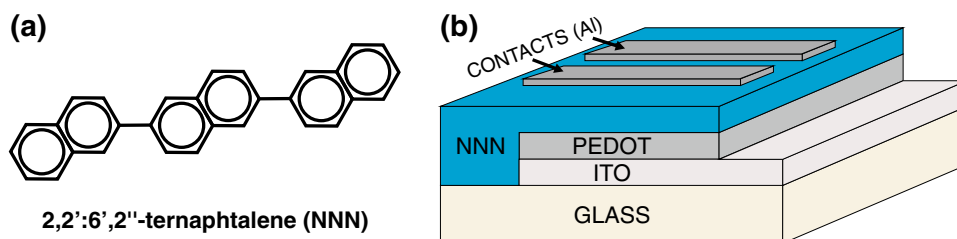


**Fig. 2** **a** Electroluminescence spectra of a NNN OLED at various drive current levels. **b** Current voltage characteristics of the device. **c** Contour plot of the emission intensity depending on wavelength and current. **d** CIE color map showing the emission color of the device at

various current levels. **e** Image of the operating device: the emission area is defined by patterning the top Al contact (shadow mask deposition) and the width of the broader line (right) is 0.5 mm

## 2.2 Device preparation

The first step in preparing the OLED device was to spin coat poly[3,4-(ethylenedioxy) thiophene]:poly(styrene sulfonate) (PEDOT:PSS) on Indium Tin Oxide (ITO)-covered glass as an anode contact. Thereafter, samples have been inserted into the NNN deposition chamber and they have been preheated to the growth temperature for 30 min to clean the surface from adsorbents and to avoid temperature gradients during the deposition process. Next, NNN was deposited by hot wall epitaxy [22] for 60 min at a substrate temperature of 80 °C and at a base pressure of  $2 \times 10^{-6}$  mbar. Prior to deposition, NNN has been purified by a thermal sublimation procedure. The final step was the deposition of 100 nm of Al as cathode through a shadow

mask. Figure 1b shows a sketch of the fabricated OLED device.

## 2.3 Electrical and optical device characterization

For electro-optical characterization, the devices were mounted in an electrically shielded box equipped with an optical window. The measurements were performed at room temperature under ambient atmosphere. The collected EL was focused into an optical fiber coupled to a Avantes AvaSpec 2048 spectrometer with a resolution of 2.4 nm. Simultaneous to the spectral analysis, the electrical characterization was performed with a Keithley 6487 current-voltage source meter.

Images of the operating OLEDs have been acquired with a digital optical camera attached to a Nikon SMZ-2T microscope.

#### 2.4 Morphological investigation

Atomic force microscopy (AFM) studies of the deposited organic films were performed using a Digital Instruments Dimension 3100 in tapping mode. The images have been acquired at scan speeds of 4–6  $\mu\text{m/s}$  using SiC tips exhibiting a cone angle of  $40^\circ$ . Nominal values for resonance frequency and tip radius are 325 kHz and 10 nm, respectively. Data analysis was performed with the software Gwyddion [23].

#### 2.5 Structural investigation

X-Ray diffraction (XRD) measurements were carried out on a Philips X'pert X-ray diffractometer using Cr  $K\alpha$  radiation ( $\lambda = 2.29 \text{ \AA}$ ) and a secondary graphite monochromator. Specular scans were performed in Bragg–Brentano configuration by varying the z-component of the scattering vector  $q$  [24]. Consequently it is possible to detect lattice planes which are parallel to the sample surface.

The monoclinic unit cell parameters of NNN, which have been used to evaluate the measurement data, are given by  $a = 8.15 \text{ \AA}$ ,  $b = 5.98 \text{ \AA}$ ,  $c = 19.45 \text{ \AA}$  and  $\beta = 94.58^\circ$  [25].

### 3 Results and discussion

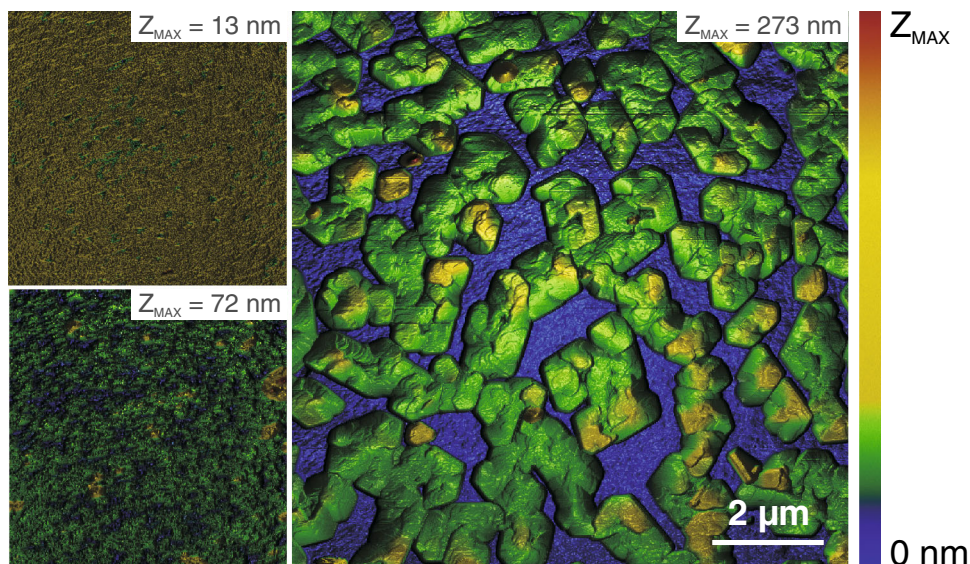
The OLEDs have been prepared and analyzed as explained in Sect. 2. As shown in Fig. 2a, c electroluminescence was

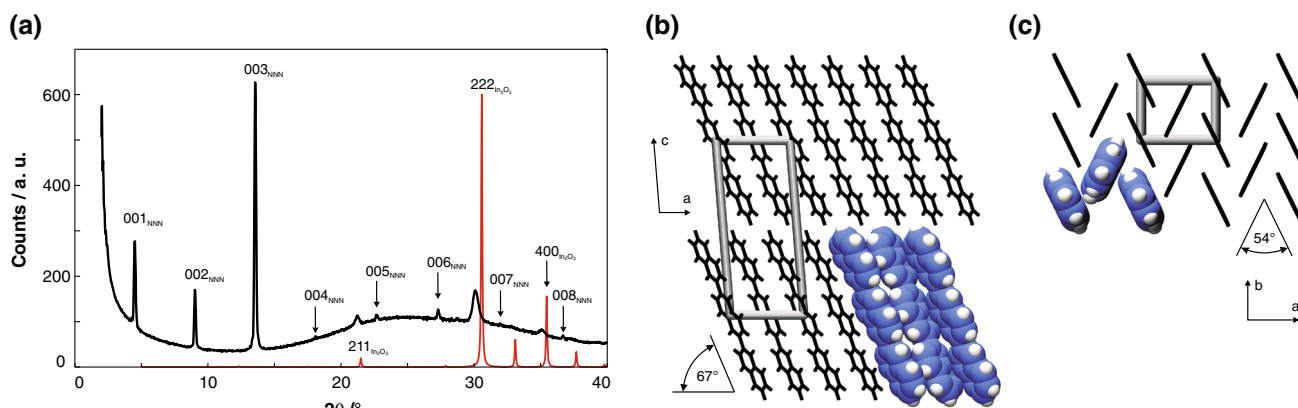
collected and spectrally analyzed in the range of 300–900 nm. An emission pattern is observable in the blue spectral range of the visible regime, with its main peaks at 383 and 405 nm and an additional shoulder at 427 nm representing the 0–0, 0–1 and 0–2 vibronic transitions, respectively. The onset of the spectral emission at 368 nm gives an estimated band gap for NNN of  $\approx 3.37 \text{ eV}$ . Spectroscopic measurements have been obtained at drive currents ranging from 0–30 mA and there is no significant shift in the positions of the emission peaks. Therefore, it can be stated that the emission color is stable in the investigated current regime. This point is further underlined by the calculation of the color coordinates of the emission according to the 1931 Commission Internationale de l'Eclairage (CIE), as depicted in Fig. 2d. Values of  $x = 0.183 \pm 0.002$  and  $y = 0.109 \pm 0.007$  have been obtained.

Figure 2b shows the current–voltage characteristics of the NNN OLED, which exhibits a clear current onset at 3.8 V and a negligible leakage current. The current onset is roughly 0.4 V above the band gap of NNN, which indicates small losses. The device homogeneity is demonstrated by the fabrication of structured Al top contacts. The light-emitting area, which is depicted in Fig. 2e, consists of a  $\approx 0.5 \times 5.5 \text{ mm}^2$  rectangle with a signature attached to it, representing the logo of our institute with a line width of 100  $\mu\text{m}$ . The image is evidence of a uniform light intensity and a homogeneous current transport, without significant indications of pinholes.

Further investigations have been carried out in relation to the morphological quality of the fabricated organic thin films. AFM images of the ITO, PEDOT and NNN surfaces are depicted in Fig. 3. The films have been prepared using the same method employed for the fabrication of the OLED device. The ITO surface is very smooth, exhibiting a rms

**Fig. 3** AFM scans of ITO on glass (*top left*), spin-coated PEDOT on top of ITO (*bottom left*) and NNN on top of PEDOT (*right*) deposited by hot wall epitaxy at  $100^\circ\text{C}$  substrate temperature. The respective maximum values for the height scale ( $Z_{\text{MAX}}$ ) are mentioned for each image





**Fig. 4** **a** Specular X-ray investigation of NNN deposited at 80 °C on top of glass–ITO–PEDOT. All observed Bragg peaks can be explained by the presence of NNN crystals and indium oxide. The red line represents a powder spectrum of  $\text{In}_2\text{O}_3$  taken from the

roughness of 1.18 nm. PEDOT layers have been deposited on top to improve band alignment and injection as reported for a similar small molecule-based OLED (*para*-hexaphenyl) [15]. The PEDOT surface exhibits a rms roughness of 7.7 nm. On top of PEDOT, the active NNN layer has been deposited and, interestingly, we do not observe a closed film using AFM but NNN molecules appear to be organized in individual crystallites with an average height of 46 nm and lateral dimensions in the order of 0.5–1  $\mu\text{m}$ . It follows, that the low leakage current of the device cannot be related to the active layer but the PEDOT layer is responsible for this observation, as PEDOT acts as an electron blocking layer.

To further study the molecular order of the crystalline NNN thin films, X-ray diffraction measurements have been performed. The peak positions in the specular scan shown in Fig. 4a can be explained by NNN crystals with their (001) net-planes parallel to the substrate surface and the respective crystal structure has been reported elsewhere [25]. The (00 $l$ ) series is indexed in the plot and the (001) reflex is observed at 4.51°. Peaks are present up to the eighth order, which reflects the high crystallographic quality of the grown thin films. (001) Contact planes of crystallites based on rodlike organic molecules prepared on isotropic substrates have been also reported for e.g., *para*-hexaphenyl [26], pentacene [27] and  $\alpha$ -sexithiophene [28]. In addition, it is possible to detect peaks which can be explained by the presence of indium oxide ( $\text{In}_2\text{O}_3$ ). It is visible, that the measured ITO peak positions are found at smaller angles as predicted by the  $\text{In}_2\text{O}_3$  powder spectrum (red line). This can be understood, because ITO is based on doping of an  $\text{In}_2\text{O}_3$  lattice (replacing  $\text{In}^{3+}$  by  $\text{Sn}^{4+}$  ions) [29] and the substitutional incorporation of Sn leads to an increased lattice constant [30, 31].

literature [37]. **b** Side view of a NNN crystal; the gray rectangle shows the *a*–*c* plane of the monoclinic unit cell. **c** Top view of the NNN crystal, with the gray rectangle showing the *a*–*b* plane of the unit cell

A real space model of the molecular orientation is presented in Fig. 4b, c which can be derived from the crystallographic unit cell and the crystal contact plane. The side view (cut through the *a*–*c* plane of the NNN crystal) shows that the molecules are aligned almost perpendicular to the substrate. The long molecular axis is tilted with respect to the substrate surface by a value of 67°. The cut through the *a*–*b* plane of the NNN crystal (top view) shows that the molecular planes (defined by common planes of naphthalene units) of adjacent molecules are rotated by 54°. The so-called herringbone packing is commonly observed in rodshaped all-aromatic planar molecules like *para*-hexaphenyl [26],  $\alpha$ -sexithiophene [32] or pentacene [33].

It has to be stated, that an upright standing orientation of a rodlike chromophore is not optimized for OLED emission as reported by Yanagi and Okamoto [34] for the example of *para*-hexaphenyl. This is caused by the alignment of the optical transition dipole, which is typically parallel to the long molecular axis [34, 35, 36].

## 4 Conclusions

OLEDs have been prepared on the basis of 2,2':6',2''-ter-naphthalene (NNN) as a non-doped emitter. Electro-optical characterization showed homogeneous deep-blue emission, exhibiting CIE color coordinates of  $x = 0.18$  and  $y = 0.11$ , which is close to the National Television System Committee (NTSC) blue color standard ( $x = 0.14$  and  $y = 0.08$ ) [15]. In addition, color stability, low losses and a low leakage current of the device could be demonstrated. Interestingly, the NNN thin film is not composed of a closed layer, but of individual (001)-oriented crystals consisting of standing molecules (tilt angle 23° with

respect to the layer normal) packed in a herringbone structure.

**Acknowledgments** This work has been financially supported by the Austrian Science Fund (FWF Projects NFN-S9706 and P25154-N20) and by the federal government of Upper Austria (project Organische Nanostrukturen). The authors thank H. Peirlberger for a CAD construction of the HWE setup.

**Open Access** This article is distributed under the terms of the Creative Commons Attribution License which permits any use, distribution, and reproduction in any medium, provided the original author(s) and the source are credited.

## References

1. C.W. Tang, S.A. VanSlyke, *Appl. Phys. Lett.* **51**(12), 913 (1987). doi:[10.1063/1.98799](https://doi.org/10.1063/1.98799)
2. C. Adachi, T. Tsutsui, S. Saito, *Appl. Phys. Lett.* **55**(15), 1489 (1989). doi:[10.1063/1.101586](https://doi.org/10.1063/1.101586)
3. C.W. Tang, S.A. VanSlyke, C.H. Chen, *J. Appl. Phys.* **65**(9), 3610 (1989). doi:[10.1063/1.343409](https://doi.org/10.1063/1.343409)
4. C. Adachi, T. Tsutsui, S. Saito, *Appl. Phys. Lett.* **56**(9), 799 (1990). doi:[10.1063/1.103177](https://doi.org/10.1063/1.103177)
5. S. Reineke, F. Lindner, G. Schwartz, N. Seidler, K. Walzer, B. Lussem, K. Leo, *Nature* **459**, 234 (2009). doi:[10.1038/nature08003](https://doi.org/10.1038/nature08003)
6. N. Thejo Kalyani, S. Dhoble, *Renew. Sust. Energ. Rev.* **16**(5), 2696 (2012). doi:[10.1016/j.rser.2012.02.021](https://doi.org/10.1016/j.rser.2012.02.021)
7. H. Sasabe, J. Kido, *J. Mater. Chem. C* **1**, 1699 (2013). doi:[10.1039/C2TC00584K](https://doi.org/10.1039/C2TC00584K)
8. K. Chung, N. Kim, J. Choi, C. Chu, J.m. Huh, *SID Symp. Dig. Tech.* **37**(1), 1958 (2006). doi:[10.1889/1.2451418](https://doi.org/10.1889/1.2451418)
9. H.D. Kim, J.K. Jeong, H.J. Chung, Y.G. Mo, *SID Symp. Dig. Tech.* **39**(1), 291 (2008). doi:[10.1889/1.3069649](https://doi.org/10.1889/1.3069649)
10. M. Zhu, C. Yang, *Chem. Soc. Rev.* **42**, 4963 (2013). doi:[10.1039/C3CS35440G](https://doi.org/10.1039/C3CS35440G)
11. G. Leising, S. Tasch, C. Brandstatter, F. Meghdadi, G. Froyer, L. Athouel, *Adv. Mater.* **9**(1), 33 (1997). doi:[10.1002/adma.19970090105](https://doi.org/10.1002/adma.19970090105)
12. H. Yanagi, T. Morikawa, S. Hotta, *Appl. Phys. Lett.* **81**(8), 1512 (2002). doi:[10.1063/1.1502023](https://doi.org/10.1063/1.1502023)
13. S.W. Wen, M.T. Lee, C.H. Chen, *J. Disp. Technol.* **1**(1), 90 (2005). doi:[10.1109/JDT.2005.852802](https://doi.org/10.1109/JDT.2005.852802)
14. L. Wang, Y. Jiang, J. Luo, Y. Zhou, J. Zhou, J. Wang, J. Pei, Y. Cao, *Adv. Mater.* **21**(47), 4854 (2009). doi:[10.1002/adma.200901039](https://doi.org/10.1002/adma.200901039)
15. C. Simbrunner, G. Hernandez-Sosa, E. Baumgartner, G. Hesser, J. Roither, W. Heiss, H. Sitter, *Appl. Phys. Lett.* **94**, 073505 (2009). doi:[10.1063/1.3086295](https://doi.org/10.1063/1.3086295)
16. J. Kjelstrup-Hansen, X. Liu, H.H. Henrichsen, K. Thilising-Hansen, H.G. Rubahn, *Phys. Status Solidi C* **7**(11–12), 2763 (2010). doi:[10.1002/pssc.200983812](https://doi.org/10.1002/pssc.200983812)
17. X. Liu, J. Kjelstrup-Hansen, H. Boudinov, H.G. Rubahn, *Org. Electron.* **12**(10), 1724 (2011). doi:[10.1016/j.orgel.2011.07.002](https://doi.org/10.1016/j.orgel.2011.07.002)
18. T. Griesser, S.V. Radl, T. Koeplmayr, A. Wolfberger, M. Edler, A. Pavitschitz, M. Kratzer, C. Teichert, T. Rath, G. Trimmel, G. Schwabegger, C. Simbrunner, H. Sitter, W. Kern, *J. Mater. Chem.* **22**, 2922 (2012). doi:[10.1039/C1JM14100G](https://doi.org/10.1039/C1JM14100G)
19. A. Montaigne Ramil, G. Hernandez-Sosa, T. Griesser, C. Simbrunner, T. Hoefler, G. Trimmel, W. Kern, Q. Shen, C. Teichert, G. Schwabegger, H. Sitter, N.S. Sariciftci, *Appl. Phys. A Mater.* **107**(4), 985 (2012). doi:[10.1007/s00339-012-6853-2](https://doi.org/10.1007/s00339-012-6853-2)
20. M. Ullah, K. Tandy, S.D. Yambem, M. Aljada, P.L. Burn, P. Meredith, E.B. Namdas, *Adv. Mater.* (2013). doi:[10.1002/adma.201302649](https://doi.org/10.1002/adma.201302649)
21. C. Simbrunner, G. Schwabegger, R. Resel, T. Dingemans, H. Sitter, *Cryst. Growth Des.* **14**(2), 442 (2014). doi:[10.1021/cg400912t](https://doi.org/10.1021/cg400912t)
22. H. Sitter, A. Andreev, G. Matt, N. Sariciftci, *Synth. Met.* **138**, 9 (2003). doi:[10.1016/S0379-6779\(02\)01306-1](https://doi.org/10.1016/S0379-6779(02)01306-1)
23. D. Nečas, P. Klapetek, *Cent. Eur. J. Phys.* **10**, 181 (2012). doi:[10.2478/s11534-011-0096-2](https://doi.org/10.2478/s11534-011-0096-2)
24. J. Brentano, *Proc. Phys. Soc. London* **37**(1), 184 (1924). doi:[10.1088/1478-7814/37/1/326](https://doi.org/10.1088/1478-7814/37/1/326)
25. A. Pichler, R. Resel, A. Neuhold, T. Dingemans, G. Schwabegger, M. Moret, C. Simbrunner, I. Salzmann, *Z. Kristallogr.* (2014). doi:[10.1515/zkri-2013-1704](https://doi.org/10.1515/zkri-2013-1704)
26. R. Resel, *J. Phys. - Condens. Mat.* **20**(18), 184009 (2008). doi:[10.1088/0953-8984/20/18/184009](https://doi.org/10.1088/0953-8984/20/18/184009)
27. D.J. Gundlach, T.N. Jackson, D.G. Schlom, S.F. Nelson, *Appl. Phys. Lett.* **74**(22), 3302 (1999). doi:[10.1063/1.123325](https://doi.org/10.1063/1.123325)
28. B. Servet, G. Horowitz, S. Ries, O. Lagorsse, P. Alnot, A. Yassar, F. Deloffre, P. Srivastava, R.a. Hajlaoui, *Chem. Mater.* **6**(10), 1809 (1994). doi:[10.1021/cm00046a039](https://doi.org/10.1021/cm00046a039)
29. H. Köstlin, R. Jost, W. Lems, *Phys. Status Solidi A* **29**(1), 87 (1975). doi:[10.1002/pssa.2210290110](https://doi.org/10.1002/pssa.2210290110)
30. M. Quaas, C. Eggs, H. Wulff, *Thin Solid Films* **332**, 277 (1998). doi:[10.1016/S0040-6090\(98\)01064-5](https://doi.org/10.1016/S0040-6090(98)01064-5)
31. R. Kleinhempel, G. Kaune, M. Herrmann, H. Kupfer, W. Hoyer, F. Richter, *Microchim. Acta* **156**(1–2), 61 (2006). doi:[10.1007/s00604-006-0591-0](https://doi.org/10.1007/s00604-006-0591-0)
32. G. Horowitz, B. Bachet, A. Yassar, P. Lang, F. Demanze, J.L. Fave, F. Garnier, *Chem. Mater.* **7**, 1337 (1995). doi:[10.1021/cm00055a010](https://doi.org/10.1021/cm00055a010)
33. J. Cornil, J.P. Calbert, J.L. Bredas, *J. Am. Chem. Soc.* **123**(6), 1250 (2001). doi:[10.1021/ja005700i](https://doi.org/10.1021/ja005700i)
34. H. Yanagi, S. Okamoto, *Appl. Phys. Lett.* **71**(18), 2563 (1997). doi:[10.1063/1.119331](https://doi.org/10.1063/1.119331)
35. F. Kouki, P. Spearman, P. Valat, G. Horowitz, F. Garnier, *J. Chem. Phys.* **113**(1), 385 (2000). doi:[10.1063/1.481804](https://doi.org/10.1063/1.481804)
36. G. Weiser, S. Möller, *Phys. Rev. B* **65**, 045203 (2002). doi:[10.1103/PhysRevB.65.045203](https://doi.org/10.1103/PhysRevB.65.045203)
37. W.H. Zachariasen, *Geol. Foren. Stock. For.* **51**(1), 123 (1929). doi:[10.1080/11035892909447062](https://doi.org/10.1080/11035892909447062)